INSTITUTE OF THEORETICAL
AND EXPERIMENTAL PHYSICS

61–89

V.S.Popov, V.D.Mur, A.V.Sergeev,
A.V.Shcheblykin

THE STARK EFFECT IN INTENSE FIELD FOR THE RYDBERG STATES

Moscow — [redacted]INFORM — 1989

УДК 539.I M-I6

THE STARK EFFECT IN INTENSE FIELD FOR THE RYDBERG STATES: Preprint ITEP 89-61/

V.S.Popov, V.D.Mur, A.V.Sergeev, A.V.Shcheblykin - M.: ATOMINFORM, 1989 - 36p.

The Stark shifts and widths of atomic states in an intense electric field $\mathcal{E}$ are calculated up to $n^4\mathcal{E} \sim 1$. Two independent calculation methods are used: summation of perturbation series and 1/n-expansion. The scaling relations for hearthreshold Stark resonances with quantum numbers $n_1 \sim n \gg 1$, n_2 and $m \sim 1$ are obtained which are in a good agreement with available experimental data for hydrogen, sodium and rubidium.

Fig. - 7, ref. - 29

1. Nearthreshold resonances in atomic photoionization cross sections in the presence of strong electric field have been investigated in many experiments (see [1-6] and references therein). The energies and widths of these resonances coincide with a high degree of accuracy with the complex energies $E^{(n_1 n_2 m)} = E - i\Gamma/2$ of the Stark quasistationary states [7,8]. To calculate them we use two independent methods: summation of divergent perturbation theory (PT) series [9,10] and 1/n-expansion [11,12]. The basic results of our computations for the Rydberg $(n \gg 1)$ states in a hydrogen atom are discussed below. Using the quantum defect method [13,14] we generalize the theory to the Rydberg states of an arbitrary atom in a strong field (up to values $\mathcal{E} \sim n^{-4}$ comparable with atomic field at the corresponding electron orbit) and obtain scaling relations for nearthreshold resonances. All the results can be verified experimentally.

If not specified we use atomic units, $\hbar = m_e = e = 1$, and reduced variables

$$F = n^4 \mathcal{E}, \quad \epsilon = 2n^2 E^{(n_1 n_2 m)} = \epsilon' - i\epsilon'', \quad \epsilon'' = n^2 \Gamma^{(n_1 n_2 m)}$$

n_1, n_2 and m are parabolic quantum numbers $(m \geq 0)$, $n = n_1 + n_2 + m + 1$ - the principal quantum number.

2. Summation of perturbation series The PT coefficients ϵ_k for the Stark problem in a hydrogen atom,

$$\epsilon^{(n_1 n_2 m)}(F) = \sum_{k=0}^{\infty} \epsilon_k F^k, \qquad (1)$$

can be readily obtained using the recurrence relations [15-18], e.g., ϵ_k up to k=160 were computed for the case of ground state [16]. The coefficients ϵ_k grow factorially at $k \to \infty$ and therefore the series (1) is not convergent but only asymptotic.

Different methods were used for summation of divergent PT series in quantum mechanics (anharmonic oscillator, the Yukawa and funnel potentials etc.), namely Padé approximants (PA), Padé-Borel transformation etc. An additional difficulty arises in the case of the Stark effect: the constant sign divergent series are to be summed. When calculating the energy $E^{(n_1 n_2 m)}$ using the coefficients $\epsilon_k^{(n_1 n_2 m)}$ we consider the two states $|n_1 n_2 m\rangle$ and $|n_2 n_1 m\rangle$ simultaneously, and define the functions

$$\epsilon_+(F^2) = \frac{1}{2}\left[\epsilon^{(n_1 n_2 m)}(F) + \epsilon^{(n_2 n_1 m)}(F)\right] = \sum_{j=0}^{\infty} \epsilon_{2j}^{(n_1 n_2 m)} F^{2j}$$

$$\epsilon_-(F^2) = \frac{1}{2F}\left[\epsilon^{(n_1 n_2 m)}(F) - \epsilon^{(n_2 n_1 m)}(F)\right] = \sum_{j} \epsilon_{2j+1}^{(n_1 n_2 m)} F^{2j} \qquad (2)$$

which have an essential singularity at F=0 and the cut $0 < F^2 < \infty$ (note that $\epsilon^{(n_1 n_2 m)}(F) = \epsilon_+(F^2) + F\epsilon_-(F^2)$).

In this case the Hermite-Padé approximants (HPA) appeared to be an effective method for summing PT. The HPA value $y(F^2) \equiv [L, M, N](F^2)$ is the solution of the equation $P_L(F^2) - Q_M(F^2)y + R_N(F^2)y^2 = 0$ where P_L, Q_M and R_N are polynomials of degrees L, M and N. Their coefficients are uniquely defined by the condition

$$P_L - Q_M \epsilon_\pm + R_N \cdot (\epsilon_\pm)^2 = O\left(F^{2(L+M+N+2)}\right), \qquad (3)$$
$$F \to 0,$$

where $\epsilon_{\pm}(F^2)$ are defined by the PT expansions (2).

We computed usually successively HPA's (L,L,L), (L+1,L,L) (L+1,L+1,L), etc. The study of their convergence with growing L has shown that the numerical values of HPA stabilize at L=10÷12 and the accuracy $\sim 10^{-3} \div 10^{-4}$ in the energy computation is achieved (up to $F \lesssim 0.3$ for the ground state $|0,0,0\rangle$ and $F<1$ for excited states). In this case 6 L + 4 $\sim$ 60÷80 orders of PT are introduced into computation. In the weak field region this procedure defines the imaginary part of the energy, $\epsilon_n'' = n^2 \Gamma^{(n_1 n_2 m)}$, only when it exceeds 10^{-8}. For further calculation details see refs.[10,19].

The above method made it possible to compute $E_{\pm}^{(n_1 n_2 m)}$ and widths $\Gamma^{(n_1 n_2 m)}$ for different states $|n_1, n_2, m\rangle$ of a hydrogen atom (the results obtained can be found in refs.[10,11, 19]). As an illustration we give in Fig.1 the trajectories of the Stark resonances in the complex plane of the reduced energy $\epsilon_n = \epsilon' - i\epsilon''$ for states with n=1,2 and 3.

3. 1/n-expansion for the energy is

$$\epsilon^{(n_1 n_2 m)}(F) = \epsilon^{(0)} + \frac{\epsilon^{(1)}}{n} + \frac{\epsilon^{(2)}}{n^2} + \cdots \qquad (4)$$

The first term $\epsilon^{(0)}$ corresponds to the $n \to \infty$ limit and can be calculated with the help of the WKB method[10]. The computation of the coefficients $\epsilon^{(k)}$ for $|0,0,n-1\rangle$ states (which correspond to the circular electron orbits perpendicular to the $\mathcal{E}$ direction) is reduced to the solution of algebraic equations. The first coefficients $\epsilon^{(0)}$, $\epsilon^{(1)}$ and $\epsilon^{(2)}$ were obtained analytically[11] while the next $\epsilon^{(k)}$ were computed numerically

by recurrence relations [12]. While the PT coefficients ϵ_k start growing from k=0, the 1/n-expansion coefficients $\epsilon^{(k)}$ first decrease by 2-3 orders of magnitude (up to $k \sim 5$) and begin to increase only at $k \gtrsim 10$. That is why the series (4) can be summed with a higher accuracy than the PT series (1), especially for the Rydberg states.

For the m=0 states the integrals entering the Bohr-Sommerfeld quantization condition can be calculated analytically. We included also the correction due to finite barrier penetrability in the effective potential $U_2(\eta) = \frac{n^2-1}{8\eta^2} - \frac{\beta_2}{2\eta} - \frac{1}{8}\mathcal{E}\eta$. The Schrödinger equation near the barrier summit $\eta = \eta_m$ $(\eta = z - z_m)$ allows an exact solution in the parabolic cylinder functions, which is matched with the quasiclassical wave function at $\eta < \eta_m$, while with $\eta \to \infty$ the solution goes over into an outgoing wave (the quasistationary state). As a result, we get the equations [1]

$$\beta_1(-\epsilon)^{-1/2} f(z_1) \simeq \nu_1,$$
$$\beta_2(-\epsilon)^{-1/2} f(z_2) = \nu_2 - \frac{1}{2\pi n}\varphi(a), \qquad (5)$$

where β_i are separation constants, $\beta_1 + \beta_2 = 1$, $\nu_i = (n_i + \frac{1}{2})/n$, $z_i = (-1)^i 16\beta_i F/\epsilon^2$, i =1 and 2, $f(z) = F(1/4, 3/4; 2; z)$ is the hypergeometric function,

$$\varphi(a) = \frac{1}{2i}\ln\left\{\frac{\Gamma(\frac{1}{2}+ia)}{\Gamma(\frac{1}{2}-ia)(1+e^{-2\pi a})}\right\} + a(1-\ln a) \qquad (5')$$

and

$$a = \frac{1}{\pi}\int_{\eta_1}^{\eta_2}\left(-p_\eta^2\right)^{1/2}d\eta = \frac{n(-\epsilon)^{3/2}}{2^{3/2}F}(1-z_2)f(1-z_2) \qquad (6)$$

($z_1 < \eta < \eta_2$ is the subbarrier region).

Hence, the well-known PT expansion[15] for $\epsilon^{(n_1 n_2 0)}$ follows from (5). In this case $a \to \infty$,

$$a = \frac{n}{3\pi F} + \frac{2n_2+m+1}{2\pi}\ln F + O(1),$$
$$\varphi(a) = \frac{1}{24a} + \frac{7}{2880a^3} + \cdots + \frac{i}{2}e^{-2\pi a} + \cdots \qquad (7)$$

Taking into account exponentially small imaginary part of $\varphi(a)$ in eqs.(5) one can easily obtain the weak-field behaviour[14,15]

$$\Gamma^{(n_1 n_2 m)} \sim F^{-(2n_2+m+1)}\exp\left(-2n/3F\right) \quad \text{at } F \to 0,$$

see Sect.3 in Appendix A.

At $F \neq 0$ eqs.(5) can be solved only numerically.

Very exact numerical calculations of energy levels and widths in a hydrogen atom have been previously made by Damburg and Kolosov[21,14]. We compare the values of $\gamma = \left(-2E_z\right)^{-1/2}$ and Γ obtained with our methods with the corresponding values from refs.[21,14] for some states with m=0, $n_1=n_2 = (n-1)/2$ (see Table 1). The agreement between all three methods is very good that, in particular, confirms the chosen summation procedure of divergent PT series.

4. For atoms other than hydrogen the potential V(r) differs from the Coulomb potential at $z \lesssim z_a$ which is much less than the mean radius of the Rydberg states $\overline{z} \sim n^2$ (z_a is the radius of atomic core). Since the Stark shifts of the atomic levels considerably exceed the fine structure splittings, n_1, n_2

and m are good quantum numbers. In the Coulomb field there exists the well-known "accidental" degeneracy of states ($\ell = 0,1,\ldots n-1$) which is described by the hidden symmetry group SO(4) = SO(3) $\otimes$ SO(3). Its generators are the angular momentum $\vec{L}$ and the Runge-Lenz vector $\vec{A}$, while $\vec{J}_{1,2} = \frac{1}{2}(\vec{L} \pm \vec{A})$ are generators of both SO(3) subgroups. Since $\vec{L} = \vec{J}_1 + \vec{J}_2$, the transition from the parabolic basis $|n_1 n_2 m\rangle$ to the spherical one $|n\ell m\rangle$ is equivalent[23] to the coupling of two angular momenta $j_1 = j_2 = (n-1)/2$. Hence

$$\delta(n_1 n_2 m) = \frac{1}{n} \sum_{\ell=m}^{n-1} (2\ell+1) \left(C^{JM}_{j, M-m; \ell m} \right)^2 \mu_\ell \qquad (8)$$

where μ_ℓ are quantum defects for a free $(E=0)$ atom, J = (n-1)/2, M = $(n_1 - n_2 + m)/2$ and $C^{JM}_{j,M-m;\ell m}$ are the Clebsh-Gordan coefficients for the SO(3) group. The values of μ_ℓ are tabulated and sharply decrease with growing ℓ, therefore the calculation of $\delta(n_1 n_2 m)$ is not difficult [2].

Furthermore, for the states of interest ($n \gg 1$, n_2 and $m \ll n_1$) the centrifugal energy can be excluded from the quasiclassical momenta p_ξ, p_η by substituting $n_i + 1/2 \to n_i + \gamma$ into quantization rules[24] (the value of γ depends on the behaviour of the potential V(r) at the origin; in our case $\gamma = (m+1)/2$, see refs.[24,25]). As a result, we arrive at eqs.(5) with

$$\nu_i = \left(1 - \frac{\delta}{n}\right)\left(n_i + \frac{m+1}{2}\right)/n \qquad (9)$$

and $\delta = \delta(n_1 n_2 m)$. These equations are valid for the

Rydberg states of an arbitrary atom.

5. Scaling relations. At $n \to \infty$, n_2 and $m \sim 1$, eqs.(5) are reduced to one equation

$$(-\epsilon)^{1/2} = F\left(\tfrac{1}{4}, \tfrac{3}{4}; 2; -16F/\epsilon^2\right), \quad (10)$$

the solution of which is denoted by $\epsilon_{cl}(F)$. The initial terms of 1/n-expansion (4) can be expressed through the function $\epsilon_{cl}(F)$ and its derivatives, e.g.

$$\epsilon^{(1)} = p\left\{\left(1-2F\frac{d}{dF}\right)\epsilon_{cl} + \left(1-F\frac{d}{dF}\right)(-\epsilon_{cl})^{3/2}\right\},$$

$p = 2n_2 + m + 1.$

Using these formulae we may obtain the scaling relations for the nearthreshold ($E \simeq 0$) resonances. Above the ionization threshold, $E > 0$, we obtain:

$$E_z^{(n_1 n_2 m)} = \frac{1}{2\tilde{n}^2}\,\epsilon_{cl}(\tilde{n}^4\mathcal{E}), \quad \Gamma^{(n_1 n_2 m)} = \frac{p\,n_*}{n\tilde{n}^3}\,\gamma_{cl}(\tilde{n}^4\mathcal{E}) \quad (11)$$

where $\tilde{n} = n_1 + \frac{m+1}{2} - \delta$, $n_* = n - \delta$

and $\gamma_{cl}(F) = \theta(F-F_*)\cdot\left(F\frac{d}{dF} - 1\right)\epsilon_{cl}^{3/2}$ at $F > F_*$.

Note that

$$\epsilon_{cl}(F) = \begin{cases} -1 + 3F - \frac{7}{4}F^2 + \frac{33}{8}F^3 - \cdots, & F \to 0 \\ \alpha_1 f + \alpha_2 f^2 + \cdots, & F \to F_* \end{cases} \quad (12)$$

$$\gamma_{cl}(F) = \left(b_0 f^{1/2} + b_1 f^{3/2} + \cdots\right)\theta(f), \quad f = \frac{F-F_*}{F_*}$$

where [3] $F_* = 0.3834$, $\alpha_1 = 0.903$, $\alpha_2 = -0.067$, $b_0 = 1.288$ etc. 1/n-expansion defines the width Γ only at $F > F_*$. As is seen from eq.(11), for the states considered $\Gamma^{(n_1 n_2 m)} \sim 1/n^3$ in this approximation.

Below the threshold ($E < 0$) the scaling relations acquire a more complicated form [26] and will not be discussed here. It will only be mentioned that they as before contain just one universal function $\epsilon_{c\ell}(F)$ defined by eq.(10). As follows from their derivation, the relative accuracy of the scaling relations is of the order of $1/n^2$, which is quite sufficient for the Rydberg states [4]. Because of simplicity of eqs.(11), they can be used to control computations performed by more precise numerical methods.

6. As usual, the value of $\mathcal{E}$ is fixed experimentally and a sequence of resonances with given quantum numbers n_2, m is observed. It follows from eq.(11) that the $|n_1 n_2 m\rangle$ state intersects the zero-field ionization limit ($E=0$) when

$$n = n^{(0)} = k\,\mathcal{E}^{-1/4} + n_2 + \frac{m+1}{2} + \delta(n_1 n_2 m) \qquad (13)$$

where $k = 0.787$ in atomic units and $k = 37.5$ if $\mathcal{E}$ is measured in kV/cm.

Among the Stark resonances with given n the states $|n-1,0,0\rangle$ are the most long-lived. E.g., at m=0 the ratio $R = \Gamma^{(n_1 n_2 0)}(\mathcal{E}) : \Gamma^{(n-1,0,0)}(\mathcal{E})$ is

$$R \approx \begin{cases} \left[\frac{1}{n_2!}\left(\frac{0.199\,n}{F}\right)^{n_2}\right]^2, & F \ll F_* \\ 2n_2 + 1, & F > F_* \end{cases} \qquad (14)$$

The last value follows from (11) and is in agreement with numerical computations[8,19] performed by HPA for $n_2=0$ and 1.

The spacings between adjacent resonances in the $F \sim F_*$, $E \gtrsim 0$ region is[4,27]: $\Delta E = c\, \mathcal{E}^{3/4}$, $c = (\pi\gamma/2)^{1/2} = 3.708$. From the condition $\Gamma \approx \Delta E$ one can estimate the value $n=n_c$ when the adjacent resonances begin to substantially overlap and the structure in the photoionization cross-section disappears. For the number of resonance peaks in the $E > 0$ region we obtain

$$\Delta n = n_c - n^{(0)} \approx k_1 \mathcal{E}^{-1/4}, \qquad (15)$$

where $k_1 = 0.332$ for the $|n-1,0,0\rangle$ states, $k_1 = 0.043$ for the $|n-2,1,0\rangle$ states, and so on. As n_2 and m increase, the width $\Gamma^{(n_1 n_2 m)}(\mathcal{E})$ grows, while the number of resonance peaks which can be experimentally observed in the abovethreshold region decreases, correspondingly.

7. Comparison with experiment. Recently, investigation of Rydberg states of atoms and molecules attracted a great interest and significant results were obtained[14]. The energies E_z and widths Γ of subthreshold resonances in a hydrogen atom are presented in[5]. Two series of the resonances, $n_1 \gg n_2$ ("blue states") and $n_1 \lesssim n_2$ ("red states") are given in Table 3. The theoretical values of $E_z^{(n_1 n_2 m)}$ and $\Gamma^{(n_1 n_2 m)}$ were calculated by two independent methods described above (see Sec.2 and 3) which are in a good agreement. The agreement between theory and experiment is also highly satisfactory (for rubidium and sodium the values of $-E_z^{(n_1 n_2 m)}$ are given in Table 3).

In Fig.3 the energies E_2 of the Stark resonances we calculated are compared with the experimental photoionization spectrum of Na taken from ref.[2]. It is seen that the maxima in the spectrum are in in accordance with the resonance positions $E_2^{(n_1 n_2 m)}$.

The validity of the scaling relation (11) is illustrated in Fig.4. The notations of the experimental points are:

○ - $|n_1,0,0\rangle$ states in a hydrogen atom,[4] $\mathcal{E}$ =6.5 and 8.0 kV/cm;

□ - $|n_1,0,1\rangle$ and $|n_1,1,0\rangle$ states in hydrogen[4];

\+ - the data for Rb[1] ($\mathcal{E}$ = 2.189, 4.335 and 6.416 kV/cm);

✱ - $|n_1,0,0\rangle$ states for Na[2,3] at $\mathcal{E}$ = 2.15 and 4.46 kV/cm, n = 20 ÷ 35).

As for the resonance widths, the experimental points[4,5] at $F > 0.5$ are set onto universal curve according to eq.(11), see Fig.5. However, at smaller values of F there are considerable deviations from scaling due to the effect of the barrier of penetrability. The numerical solution of eqs.(5) yields correct interpolation between the weak field region and the scaling region $F > F_*$, as seen from Fig.3 agrees with experiment. It is noteworthy that the term $\varphi(a)$ in (5) is of a little importance in the $F > F_*$ region.

The number of experimental points in Figs.4,5 could be easily increased. In all the cases considered the agreement between theory and experiment is good and leaves no doubt that the peaks in photoionization cross sections correspond to the Stark quasistationary states in homogeneous electric field $\mathcal{E}$. The sca-

ling relations are applicable to the Rydberg states of an arbitrary atom and can be used to identify the quantum numbers (n_1, n_2, m) for the above peaks.

The authors are very grateful to E.A.Solov'ev, V.M.Weinberg, and especially to L.P.Pitaevsky, for useful discussions and remarks.

Appendix A

We consider here the properties of the function $\varphi(a)$ defined by eq.(5').

1. Behaviuor at $|a|\to\infty$. Using the Stirling series for $\log\Gamma(z+1/2)$ we find at $Re\,a>0$:

$$\varphi(a) \approx \sum_{k=0}^{\infty} c_k\, a^{-(2k+1)}, \qquad (A.1)$$

$$c_k = (-1)^k \frac{1-2^{-(2k+1)}}{(2k+1)(2k+2)} B_{2k+2} \underset{(k\to\infty)}{\approx} \frac{(2k)!}{2\pi^2(2\pi)^{2k}}$$

where B_{2k+2} are the Bernoulli numbers. The series (A.1) is divergent but at the beginning its coefficients decrease: $c_0 = 1/24$, $c_1 = 7/2\,880$, $c_2 = 31/40\,320$, $c_3 = 5.91(-4)$ is the minimum coefficient after which c_k begin to increase: $c_5 = 1.92(-3)$, $c_{10} = 13.42$, $c_{15} = 1.52(7)$ etc. (here $(n)\equiv 10^n$, e.g. $5.91(-4) = 5.91 \times 10^{-4}$).

With the identity

$$\left[\Gamma\left(\tfrac{1}{2}-ia\right)\left(1+e^{-2\pi a}\right)\right]^{-1} = \frac{1}{2\pi}\, e^{\pi a}\, \Gamma\left(\tfrac{1}{2}+ia\right) \qquad (A.2)$$

in view, we get

$$\varphi(-iy) = i\, \ln\left\{(2\pi)^{1/2}(y/e)^{y}/\Gamma(y+1/2)\right\} \qquad (A.3)$$

($a=-iy$, $0<y<\infty$). Thus, on the semiaxis $(0,-i\infty)$ the above function is purely imaginary:

$$\varphi(-iy) = i \times \begin{cases} \frac{1}{2}\ln 2 + y\ln y + (C+2\ln 2-1)y + \cdots \\ \qquad\qquad y \to 0; \\ \frac{1}{24y} - \frac{7}{2880y^3} + \cdots, \; y \to \infty \end{cases} \tag{A.4}$$

(C = 0.5772 ... is Euler's constant). It follows from eq.(A.3) that the asymptotic expansion (A.1) is valid when $-\pi < \arg a < \frac{\pi}{2}$.

Note that on the real axis, $\arg a = 0$,

$$\operatorname{Im}\varphi(a) = \frac{1}{2}\ln\left(1+e^{-2\pi a}\right) = \tag{A.5}$$

$$= \frac{1}{2}e^{-2\pi a} + \cdots, \; a \to \infty$$

The asymptotic expansion of $\varphi(a)$ at $\frac{\pi}{2} < \arg a < \pi$ can be found in the following way:

$$\varphi(a) = \frac{1}{2i}\ln\frac{\Gamma\left(\frac{1}{2}+ia\right)\left(1+e^{-2\pi a}\right)}{\Gamma\left(\frac{1}{2}-ia\right)} - a\ln a + a +$$

$$+ i\ln\left(1+e^{-2\pi a}\right) =$$

$$= -i\ln\left[\frac{(2\pi)^{1/2}(y/e)^y}{\Gamma(y+1/2)}\right] + i\ln\left(1+e^{-2\pi a}\right)$$

where $a = iy$ and eq.(A.2) was used. Since $\ln\left(1+e^{-2\pi a}\right) = -2\pi a + \cdots$, $\operatorname{Re} a < 0$, then

$$\varphi(a) \approx -2\pi i a + \sum_{k=0}^{\infty} c_k a^{-(2k+1)} \tag{A.6}$$

($|a| \to \infty$). Thus, we have determined the $\varphi(a)$

asymptotics for all $-\pi < \arg a < \pi$.

2. $\varphi(a)$ has logarithmic singularities at $a = 0$,

$$\varphi(a) = i\,\frac{\ln 2}{2} - a\ln a + O(a) \qquad (A.7)$$

and at the points

$$a = a_n = \left(n+\tfrac{1}{2}\right)i\,, \quad n = 0, 1, 2, \ldots \qquad (A.8)$$

where

$$\varphi(a) = i\left\{\ln(a-a_n) + A_n + \cdots\right\} \qquad (A.9)$$

$$A_n = \ln\left\{(2\pi)^{1/2}\, n!\,/\left[(2n+1)/2e\right]^{n+1/2}\right\} =$$

$$= \begin{cases} 1.766, & n = 0 \\ 1.811, & n = 1 \\ 1.838, & n \to \infty \end{cases}$$

($A_n = \ln 2\pi - \frac{1}{24n}$ at $n \gg 1$). This function is regular at the complex conjugate points $a = a_n^*$, since

$$\lim_{a \to -(n+\frac{1}{2})i} \Gamma\left(\tfrac{1}{2} - ia\right)\left(1 + e^{-2\pi a}\right) = \frac{2\pi}{n!}\, i^{2n+1}$$

We note also that

$$\varphi(in) + \varphi(-in) = i\ln 2 \qquad (A.10)$$

and thus the values of $\varphi(in)$ are purely imaginary. This is

no longer valid for other points of the semiaxis $a = iy$, $y > 0$:

$$\mathrm{Re}\, \varphi(iy) = \begin{cases} \pi y, & 0 < y < 1/2 \\ \pi(y-1), & 1/2 < y < \frac{3}{2}, \text{ etc.} \end{cases}$$

3. The weak field region. Using PT expansions [15,16] for $\mathcal{E}$ and β_2 we get ($F \to 0$):

$$z_2 = 8(1-x)F - 6\left(7x^2 - 8x + 1 + \frac{1}{3n^2}\right)F^2 + \cdots$$

where $m = 0$, $x = (n_1 - n_2)/n$. Considering also that

$$(1-z)f(1-z) = \frac{2^{7/2}}{3\pi}\left\{1 + \frac{3}{16}z\left[\ln z - \left(1 + 6\ln 2\right) + \cdots\right]\right\}$$

($z \to 0$), we find:

$$2\pi a = n\left\{\frac{2}{3F} + (1-x)\ln F - \right.$$
$$\left. - \left[3x + (1-x)\left(1 + 3\ln 2 - \ln(1-x)\right)\right] + \cdots\right\} \qquad (A.11)$$

The resulting approximate formula

$$\tilde{\Gamma}^{(n_1 n_2 m)} = \frac{1}{2\pi n^3} e^{-2\pi a} \qquad (A.12)$$

differs from the exact asymptotics for $\Gamma^{(n_1 n_2 m)}$ at $F \to 0$ only by an inessential numerical factor. For example, at $m=0$

$$\tilde{\Gamma}^{(n_1 n_2 0)}(\mathcal{E}) \Big/ \Gamma^{(n_1 n_2 0)}(\mathcal{E}) = \begin{cases} e/\pi = 0.865 \text{ for the ground state,} \\ 4e^3/27\pi = 0.947 \text{ for the } |0,1,0\rangle \text{ state,} \\ 1 - \dfrac{1}{12 n_2}, \text{ at } n_2 \gg 1 \end{cases} \qquad \text{(A.13)}$$

Thus, the barrier penetrability correction in the WKB quantization rules allows one to match 1/n-expansion with the well-known behaviour[15] of $\Gamma^{(n_1 n_2 n)}(\mathcal{E})$ at $\mathcal{E} \to 0$.

Note that eq.(A.11) defines only $a_1 = Re\, a$. The imaginary part of a is exponentially small at $F \to 0$,

$$Im\, a = \frac{1}{4\pi^2 F} e^{-2\pi a_1} \left[1 + O(F \ln F) \right] \qquad \text{(A.14)}$$

Eqs.(A.11),(A.14) can be used in numerical calculations as initial approximation .

The trajectories $a = a(F)$ for a few typical states $|n_1 n_2 m\rangle$ are presented in Fig.6. The transition from 1/n- to $1/n^2$ approximation[26] in eqs.(5) changes the values of a but slightly and thereby the values of the energy.

Appendix B.

Let us make a few comments on numerical solution of eqs.(5).

These equations were solved by two different methods which yielded consistent results: the first is the Newton's method and the second is the successive iterations (SI). Let us briefly summarize these methods. To this end rewrite (5) in a more simple form:

$$\left.\begin{aligned} \varphi_1(z_1, z_2) &= 0 \\ \varphi_2(z_1, z_2) &= 0 \end{aligned}\right\} \quad \text{or} \quad \vec{\varphi}(\vec{z}) = 0$$

The iterations in the Newton's algorithm are built in the following way:

$$\vec{z}^{(n+1)} = \vec{z}^{(n)} - \lambda \vec{\Delta}/\Delta, \tag{B.1}$$

where λ is a certain constant, $\lambda \sim 0.05 \div 0.5$; $\Delta = \det \tilde{\omega}$, $\tilde{\omega}$ is a matrix with elements

$$\tilde{\omega}_{ij} = \left.\frac{\partial \varphi_i}{\partial z_j}\right|_{\vec{z} = \vec{z}^{(n)}} \qquad (i, j = 1 \text{ and } 2)$$

Δ^i is determinant of the matrix $\tilde{\omega}$ derived from $\| \tilde{\omega}_{ij} \|$ by replacing j-column with $-\vec{\varphi}(\vec{z}^{(n)})$.

In the SI-method $\vec{z}^{(n+1)}$ is constructed by

$$z_j^{(n+1)} = z_j^{(n)} - \kappa_j \varphi_j(\vec{z}^{(n)}) \tag{B.2}$$

It turned out that with an appropriate choice of κ_1 and κ_2 the SI-method has the most fast convergence and for $P > 0.35$

is much better than the Newton's algorithm. For example, for the case of $|16,1,0\rangle$ state with $\mu_1 = 20$, $\mu_2 = 2$ and $F = 0.2 \div 0.25$ the SI converges at 10-15 iterations while the Newton's algorithm at 20÷30; for $F \sim 0.4$, the SI requires 150 iterations while the Newton's algorithm more than 1000. In addition, the SI does not require calculation of the derivatives matrix $\|\tilde{\omega}_{ij}\|$. Let us emphasize, however, that the speed of convergence sharply depends on choosing μ_1 and μ_2 which in turn depend on the state at hand and on the value of F (if μ_i are poorely chosen the process diverges).

Eqs.(5) contain the variable

$$\omega = \frac{\Gamma\left(\frac{1}{2}+ia\right)}{\Gamma\left(\frac{1}{2}-ia\right)\left(1+e^{-2\pi a}\right)} \qquad (B.3)$$

(under the sign of logarithm). The behaviour of ω vs.F is shown in Fig.7a. It can be seen that trajectory $\omega = \omega(F)$ intersects the semiaxis $-\infty < \omega < 0$ whereupon $2\pi i$ should be added when calculating $\ln\omega$. With further increase of F the spiral in Fig.7a winds around the branch point $\omega = 0$ (or $a = \infty$) and when calculating $\ln\omega$ one should take into account the number of rotations around this point.

As shown in Fig.7a, there is a bend of trajectory at $F \approx 0.25$ (actually, as shown in Fig.7b, this trajectory is a smooth curve). To explain this note that $a \to \infty \left(a \approx \frac{n}{3\pi F}\right)$ at $F \to 0$ and therefore

$$\omega = \exp\left\{2ia\left(\ln a - 1\right) + \frac{i}{12a} + \cdots\right\} \qquad (B.4)$$

The phase of ω reaches its minimum at $a \simeq 1$ that corresponds to alternation of rotation in trajectory $\omega(F)$. In fact, this takes place near F = 0.247 and $a = 1.04 + i\, 2.10^{-4}$.

Note finally that the hypergeometric functions entering eqs.(5) at $|z|<1$ were calculated by usual series $1+\frac{\alpha\beta}{\gamma}z+\dots$ and at $|z|>1$ with the help of transformation $z \to z^{-1}$, see eq.(2.10(2)) in ref. [28].

Footnotes

1) The accuracy of these equations can be improved using the corrections $\sim \hbar^2$ in quantization rules[20] (the formal parameter $\hbar^2$ of the quasiclassical expansion goes over into $1/n^2$ for the problem at hand).

2) Thus, δ = 0.768, 0538, 0.414 and 0.336 for $|n-1,0,0\rangle$ states in Rb (n = 20,30,40 and 50), see also Fig.2. Evidently, $\delta(n_1 n_2 m) = \mu_\ell \equiv 0$ for a hydrogen atom.

3) Using eq.(10), all the coefficients α_k and b_k can, in principle, be evaluated analytically. For example,

$$\alpha_1 = \gamma^2/27\pi\,, \quad \alpha_2 = \frac{\gamma^2}{216\pi}\left(1-\frac{\gamma^2}{48}\right),$$

$$\alpha_3 = -\frac{3}{32}\left(1-\frac{\gamma^2}{216}-\frac{\gamma^4}{6912}\right)\alpha_1\,, \quad b_0 = \gamma^3/18(3\pi)^{3/2}$$

etc , where $\gamma = \left[\Gamma(1/4)/\Gamma(3/4)\right]^2 = 8.753\,757\ldots$ (numerically, we have: $\alpha_1 = 0.9034$, $\alpha_2 = -0.0673$, $\alpha_3 = 0.0173$, $\alpha_4 = -0.0063$, ...). Since $\alpha_1 \gg |\alpha_2| > \alpha_3$, the F-dependence of $\epsilon_{c\ell}$ is nearly linear within a wide range $F \sim F_*$ which is clearly seen in Fig.3. Note that $\epsilon_{c\ell}(F)$ is real at $0 < F < \infty$ and intersects $\epsilon = 0$ at $F = F_*$ which is not a singularity for the function $\epsilon_{c\ell}(F)$. On the other hand, $\gamma_{c\ell}(F)$ has a square root singularity at $F = F_*$ and $\gamma_{c\ell}(F) \equiv 0$ at $F < F_*$.

4) This estimate is supported by computations made by other methods. See, for example, the next Table which gives the values of $-E_k^{(n_1 n_2 m)}$, cm^{-1}.

computation method	a hydrogen atom, $\mathcal{E}$ = 16.8 kV/cm			Rb, $\mathcal{E}$ =2.189 kV/cm		
$(n_1 n_2 m)$	(17,0,0)	(15,0,0)	(14,1,0)	(18,0,0)	(18,1,0)	(18,2,0)
HPA	58.2	196.7	235.3	-	-	-
1/n	58.0	196.7	235.2	288.6	247.2	216.3
scaling	57.1	196.3	233.2	288.7	247.2	216.0

Note that in the region $E < 0$ we have, instead of eq.(11),

$$E_z^{(n_1 n_2 m)} = \frac{1}{2\tilde{n}^2}\left[\epsilon_{cl}(\tilde{F}) + \eta\left(\sqrt{\tilde{F}\hat{F}}\right) - \left(\frac{\tilde{n}}{n_*}\right)^2 \eta(\hat{F})\right] \quad (11a)$$

where $\tilde{F} = \tilde{n}^4 \mathcal{E}$, $\hat{F} = n_*^4 \mathcal{E}$,

$\eta(F) = [-\epsilon_{cl}(F)]^{3/2}$ at $F > F_* = 0.3834$,

$\eta(F) \equiv 0$ at $F < F_*$ and $\epsilon_{cl}(F)$ is defined by eq. (10).

The accuracy of this approximation is illustrated in Table 2 which contains the values of $-E_z^{(n_1 n_2 m)}$ calculated by HPA, eqs. (5) and (11a) ("scaling"). The error of the scaling relation (11a) increases with p/n , compare the (17,0,0) and (14,2,0) states in hydrogen.

The last line in Table 2 contains the values of $-E_z$ calculated by eqs. (5) with $\delta \equiv 0$. It shows that account of the quantum defect $\delta = \delta(n_1 n_2 m)$ is essential, especially for rubidium.

5) Here $a = a_1 + ia_2$ and we assume $n_1 \gg n_2$. Note that this asymptotics is not accurate enough at the values of $F \sim 0.1$. For example, at $F = 0.2$ numerical computation gives $a = 2.5277 + i1.852 \times 10^{-8}$, while $a_2 = 1.6 \times 10^{-8}$ according to eq. (A.14) ($n = 20$, $|19,0,0\rangle$ state). As is seen from the improved expansion,

$$a_2 = \frac{1}{4\pi^2} e^{-2\pi a_1} \left\{ F^{-1} + \ln \frac{n}{F} + 3\left(\ln 2 - \frac{\chi}{2}\right) + \dots \right\}$$

eq. (A.14) has a per cent accuracy only when $F < 0.01$.

6) HPA - the summation of perturbation series, $\sum_k \epsilon_k F^k$, using the Hermite-Padé approximants [10]; 1/n and $1/n^2$ denote the calculation of $E = E_r - i\Gamma/2$ by solving eqs. (5), with the barrier penetrability taken into account. The agreement between these values and ref. [21] is quite well. On the other hand, the approximate formulae by Drukarev [25] have a considerable less accuracy, especially for $\Gamma^{(n_1 n_2 m)}$.

7) $\underline{m = 0}$ for all the states considered; $F = n^4 \mathcal{E}$ varies from 0.126 ($n = 14$) to 0.343 ($n = 18$), F_* is the classical ionization threshold [10] and $f = (F - F_*)/F_*$. The latter quantity shows the proximity of resonance energy $E_r^{(n_1 n_2 m)}$ to the top of potential barrier in $U_2(\eta)$ and qualitatively explains the seeming irregularity in the values of $\Gamma^{(n_1 n_2 m)}$.

Table 1

Energies and widths of the Stark resonances calculated by different methods [6]

$(n_1 n_2 m)$	(2,2,0), n = 5		(5,5,0), n = 11		(7,7,0), n = 15	
$\mathcal{E}$	1.8(-4)		1.0(-5)		3.0(-6)	
F	0.1125		0.1464		0.1519	
calculation method	ν	$\Gamma \cdot 10^6$	ν	$\Gamma \cdot 10^6$	ν	$\Gamma \cdot 10^6$
HPA [10]	4.92402	2.283	10.713	2.83	14.577	1.35
1/n	4.92385	2.22	10.7128	2.82	14.5767	1.347
$1/n^2$	4.92406	2.19	10.7127	2.80	14.5766	1.338
[21]	4.9240	2.282	10.688	2.815	14.5771	1.338
[25]	4.929	2.55	10.722	3.3	14.619	1.74

Table 1

$(n_1 n_2 m)$	(7,7,0)		(7,7,0)	
$\mathcal{E}$	2.5(-6)		2.8(-6)	
F	0.1266		0.1417	
Calculation method	$-E_r$	Γ	$-E_r$	Γ
1/n	2.30650(-3)	6.5(-10)	2.33215(-3)	1.205(-7)
$1/n^2$	2.30650(-3)	6.5(-10)	2.33216(-3)	1.20(-7)
ref. [14]	2.306497(-3)	6.63(-10)	2.332163(-3)	1.214(-7)
$(n_1 n_2 m)$	(9,0,0)		(9,0,0)	
$\mathcal{E}$	2.0(-5)		3.0(-5)	
F	0.2		0.3	
Calculation method	$-E_r$	Γ	$-E_r$	Γ
1/n	2.58401(-3)	1.67(-7)	1.5647(-3)	7.25(-5)
$1/n^2$	2.58545(-3)	1.60(-7)	1.5687(-3)	-
ref. [29]	2.58557(-3)	1.902(-7)	1.57106(-3)	7.919(-5)

Foot note: here (n) $\equiv 10^n$, e.g. 2.5(-6) $\equiv 2.5 \times 10^{-6}$. The values of $\mathcal{E}$, E_r and Γ are given in atomic units, $\nu = (-2E_r)^{-1/2}$ (thus, $\nu = n$ at $\mathcal{E} = 0$).

Table 2

The values of $-E_r^{(n_1 n_2 m)}$, cm^{-1}

A hydrogen atom, $\mathcal{E}$ = 16.8 kV/cm						
$(n_1 n_2 m)$	(17,0,0)	(16,1,0)	(15,1,0)	(15,0,0)	(14,2,0)	(14,1,0)
p/n	0.056	0.17	0,18	0.063	0.29	0,19
HPA	58,2	106,6	167,7	196,7	211.6	235.3
1/n	58.0	106.6	167.5	196,7	211.5	235,2
scaling	57.1	104.2	163.5	196,3	203.2	233.2
	Rb, $\mathcal{E}$ = 2.189 kV/cm			Na, $\mathcal{E}$ = 3,590 kV/cm		
$(n_1 n_2 m)$	(18,0,0)	(18,2,0)	(23,0,0)	25,0,0)	(25,1,0)	(25,0,1)
n	19	21	24	26	27	27
δ	0.802	0,414	0,656	0,145	0,126	0.057
1/n	288,6	216.3	132,8	35.5	31,1	22,1
scaling	288,7	216,0	132,9	35,2	31,0	22,0
1/n, 0	257.5	204.7	118,5	32.6	28.8	21.0

Table 3

Energies and halfwidths of the subthreshold Stark resonances

A hydrogen atom [7], $\mathcal{E}$ = 16.8 kV/cm						
		$-E_z$, cm^{-1}		$\Gamma/2$, cm^{-1}		
(n_1,n_2)	F_*	theor.	exp. [5]	theor.	ref. [5]	f
(17,0)	0.312	58.1	60.7	2.21	2.5	0.10
(16,1)	0.265	106.6	103.8	8.93	9.	0.29
(16,0)	0.310	123.3	126.5	0.15	0.14	-0.12
(15,1)	0.263	167.6	167.9	1.84	2.1	0.04
(15,0)	0.307	196.7	198.5	7(-4)	1.1(-4)	-0.30
(14,2)	0.236	211.5	210.1	5.64	6.6	0.16
(14,1)	0.260	235.3	238.1	0.020	0.016	-0.18
(13,2)	0.233	274.2	275.8	0.27	0.23	-0.08
(12,3)	0.214	313.8	314.8	1.29	1.6	-0.001
(13,1)	0.256	315.2	314.8	-	5(-6)	-0.35
(12,2)	0.229	349.8	351.4	1.1(-4)	1(-4)	-0.28
(11,4)	0.200	352.2	351.4	3.29	3.0	0.07
(11,3)	0.211	384.4	386.3	1.9(-3)	1.8(-3)	-0.21
(10,4)	0.197	419.1	419.2	0.025	0.032	-0.16
(0,13)	0.132	781.8	781.6	0.570	0.62	-0.05
(1,12)	0.136	750.9	751.7	0.268	0.25	-0.07
(2,11)	0.140	720.0	721.0	0.105	0.11	-0.10
(3,10)	0.145	689.1	689.1	0.034	0.04	-0.13
(5,8)	0.157	627.3	629.0	1.9(-3)	2(-3)	-0.20

Table 3

Na, $\mathcal{E}$ = 3.59 kV/cm

$(n_1 n_2 m)$	δ	$-E_r$, cm^{-1} theor.	exp.	$\Gamma/2$, cm^{-1} theor.	F_*	f
(23,0,0)	0.157	80.35	79.	~3.(-6)	0.330	-0.30
(24,0,0)	0.151	56.96	56.5	2.5(-3)	0.330	-0.17
(25,0,0)	0.145	35.52	35.5	0.15	0.331	-0.04
(26,0,0)	0.140	15.52	15.5	0.83	0.332	0.12
(22,0,1)	0.065	84.36	85.	$\sim 10^{-4}$	0.300	-0.23
(23,0,1)	0.062	61.84	63.5	3.5(-2)	0.301	-0.09
(24,0,1)	0.060	41.40	41.	0.63	0.302	0.06
(25,0,1)	0.057	22.03	22.5	2.07	0.304	0.22
(23,1,0)	0.135	70.2	70.5	0.11	0.287	-0.05
(25,1,0)	0.126	31.1	30.	3.3	0.290	0.28
(22,1,1)	0.070	75.9	76.5	0.39	0.270	0.01
(23,1,1)	0.067	56.5	56.5	2.2	0.272	0.17
(24,1,1)	0.064	37.5	35.5	4.8	0.274	0.36
(22,2,0)	0.120	83.8	84.	0.71	0.261	0.04
(23,2,0)	0.117	64.7	63.5	3.1	0.263	0.21
(24,2,0)	0.114	45.7	45.5	6.1	0.265	0.40
(25,2,0)	0.111	27.2	28.5	9.0	0.266	0.61
(24,1,0)	0.130	50.3	50.5	1.2	0.288	0.11

Table 3

Rb, $\mathcal{E}$ = 2.189 kV/cm							
$(n_1 n_2 m)$	δ	$-E_r$, cm^{-1} theor.	exp.	$(n_1 n_2 m)$	δ	$-E_r$, cm^{-1} theor.	exp.
(18,0,0)	0.802	288.6	289	(21,1,0)	0.517	159.5	160
(19,0,0)	0.768	249.0	250	(22,1,0)	0.504	136.2	136
(20,0,0)	0.737	214.6	–				
(21,0,0)	0.708	184.2	184	(16,2,0)	0.428	284.0	284
(22,0,0)	0.681	157.1	157	(17,2,0)	0.421	247.9	247
(23,0,0)	0.656	132.8	133	(18,2,0)	0.414	216.3	217
				(19,2,0)	0.407	188.2	189
(17,1,0)	0.577	284.6	286	(20,2,0)	0.400	163.2	163
(18,1,0)	0.561	247.2	247	(21,2,0)	0.393	140.6	141
(20,1,0)	0.531	185.4	185	(22,2,0)	0.386	120.2	120

Footnote: here $(n) \equiv 10^n$, δ is the quantum defect (8). Theoretical values of E_r were calculated by HPA and eqs. (5), experimental values were taken from figures in refs. [2,3](Na) and [1] (Rb), the uncertainty of E_r being $\sim 0.5 \div 1.0$ cm^{-1} .

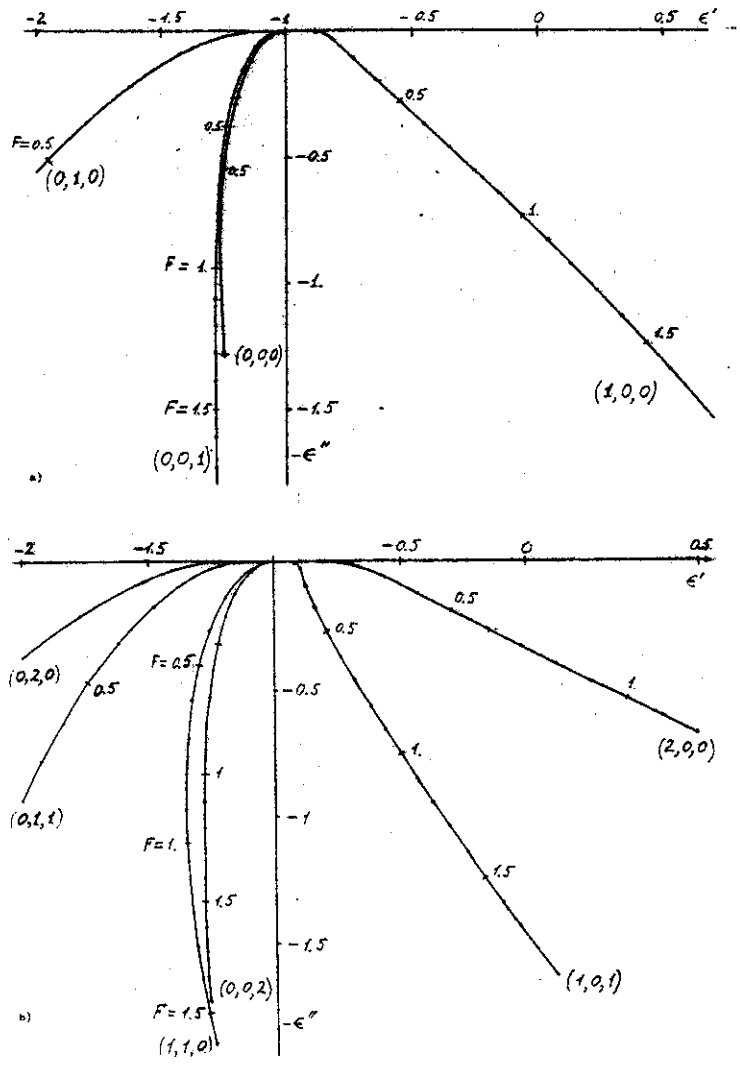

Fig.1. The trajectories of the Stark resonances in the complex plane $\epsilon = 2n^2 E^{(n_1 n_2 m)} = \epsilon' - i\epsilon''$

a) for the ground state and n=2;

b) for all the states with n=3.

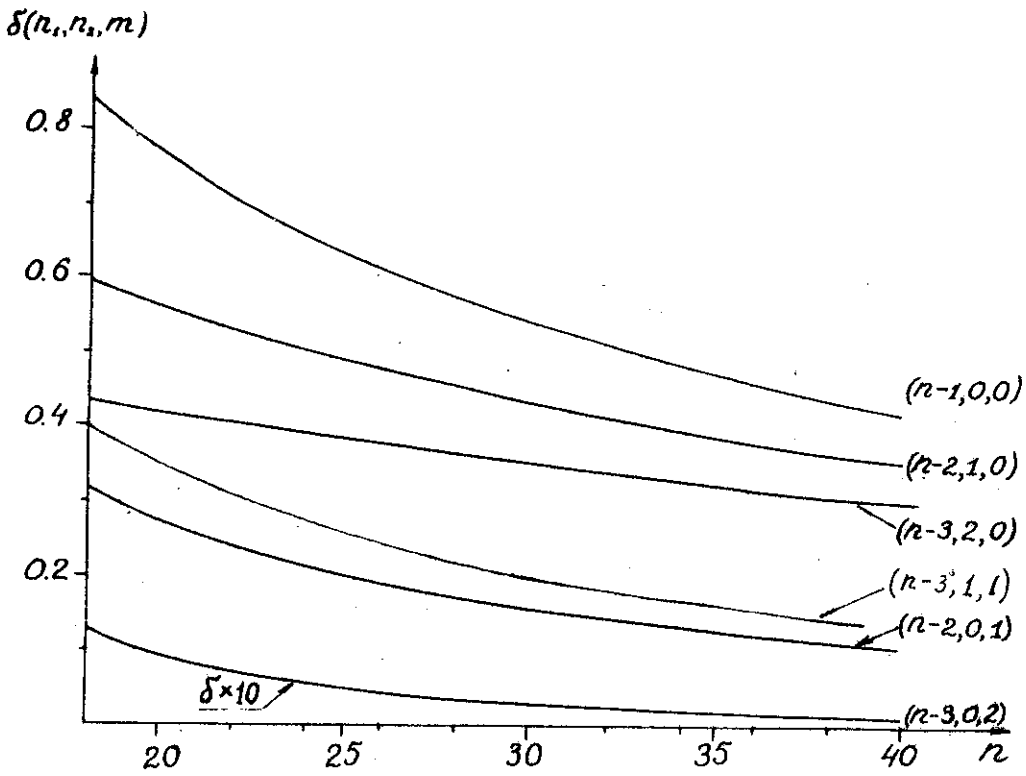

Fig. 2. The quantum defects $\delta(n_1 n_2 m)$ for a rubidium atom.

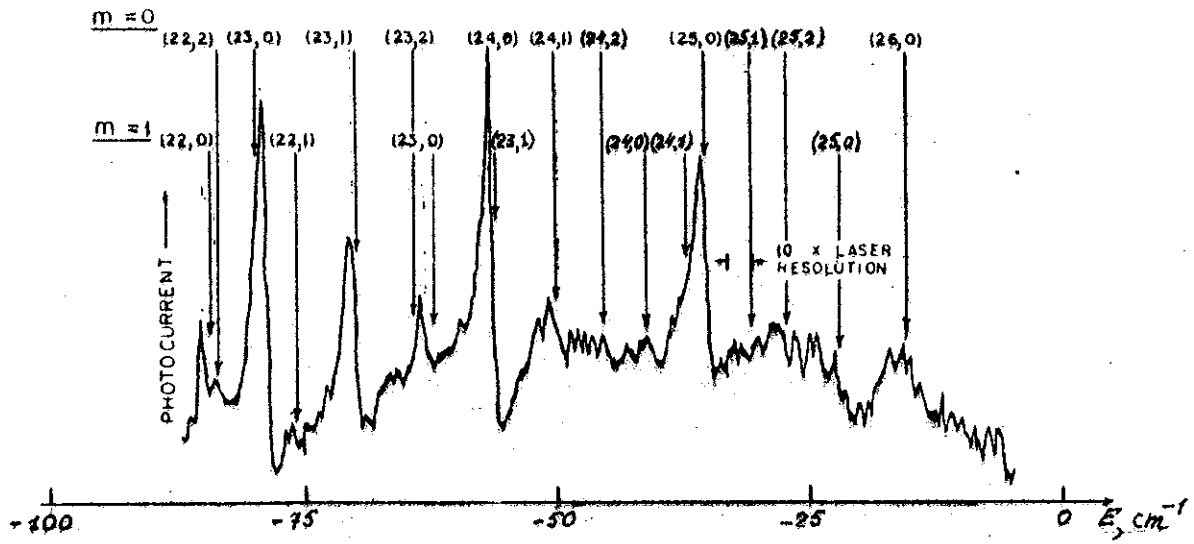

Fig.3. Photoionization cross section for Na at $\mathcal{E}$ = 3.59 kV/cm. Energies $E_2^{(n_1 n_2 m)}$ computed by eqs.(5) are shown by arrows.

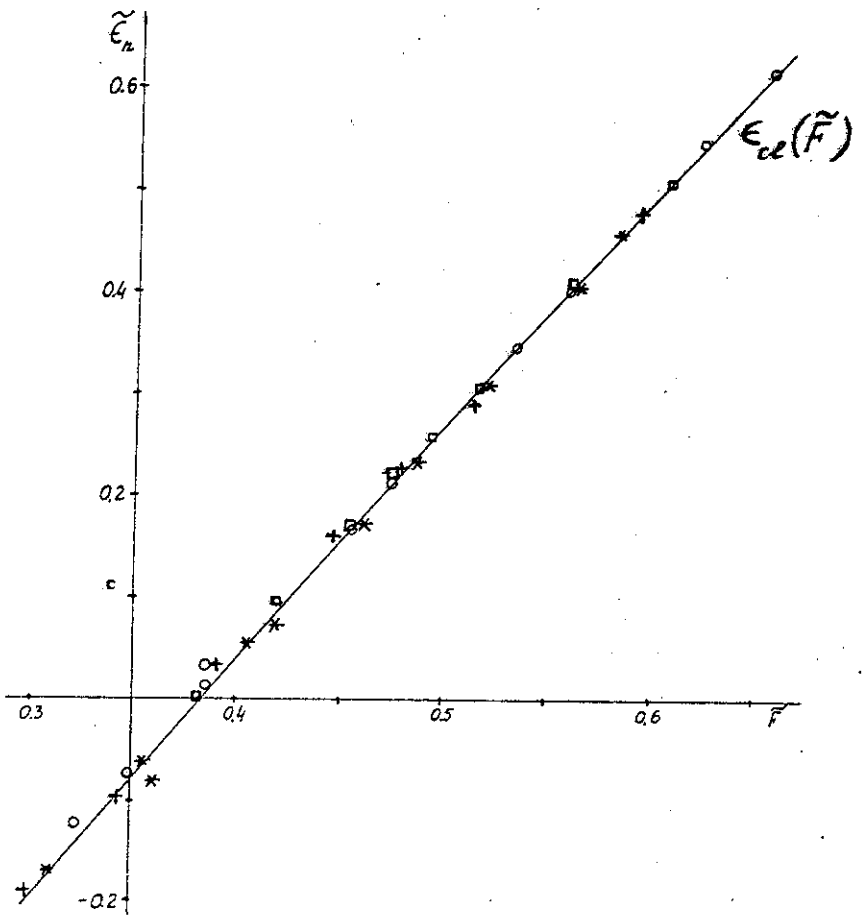

Fig.4. Scaling (11) for abovethreshold resonances. The variables $\widetilde{\epsilon}_n = 2\tilde{n}^2 E_z^{(n_1 n_2 m)}$ and $\widetilde{F} = \tilde{n}^4 \mathcal{E}$ are used, the solid curve is $\epsilon_{cl}(\widetilde{F})$. The experimental points are explained in the text.

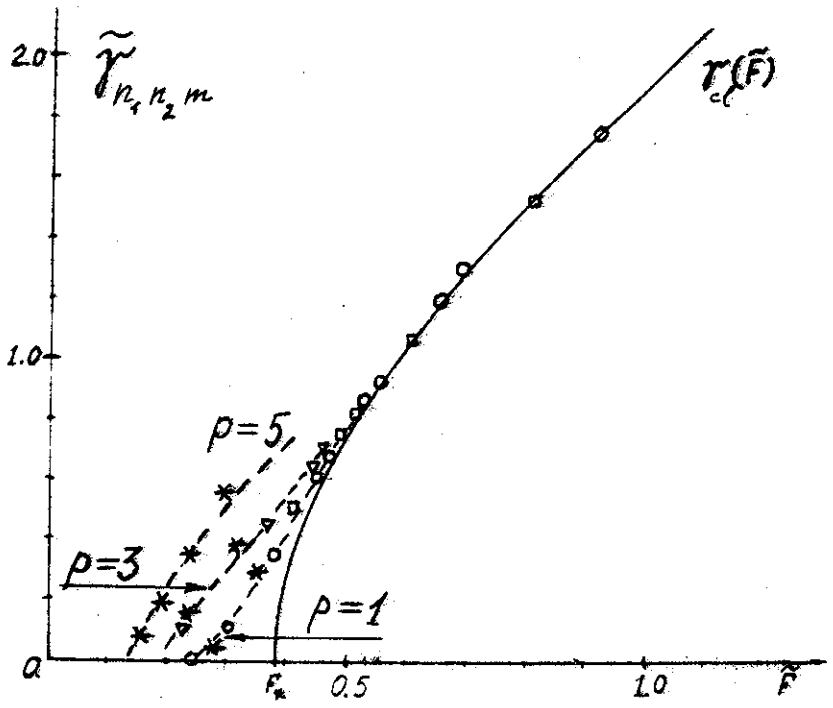

Fig.5. Scaling (11) for the widths of the Stark resonances:

$$\tilde{\Gamma}_{n_1 n_2 m} = \left(n \tilde{n}^3 / p n_*\right) \Gamma^{(n_1 n_2 m)}(\mathcal{E}),$$

$\Gamma(\mathcal{E})$ - in atomic units, $p=2n_2+m+1$ ($n = n_*$ for a hydrogen atom). Notations are:

○, □ and ▽ - $|n_1,0,0\rangle$, $|n_1,0,1\rangle$ and $|n_1,1,0\rangle$ states in hydrogen at $\mathcal{E}$=6.5 and 8.0 kV/cm [4,5], ✱ - $|n_1,n_2,0\rangle$ states in Na (n_2=0,1 and 2) at $\mathcal{E}$=3.59 kV/cm [2,3].

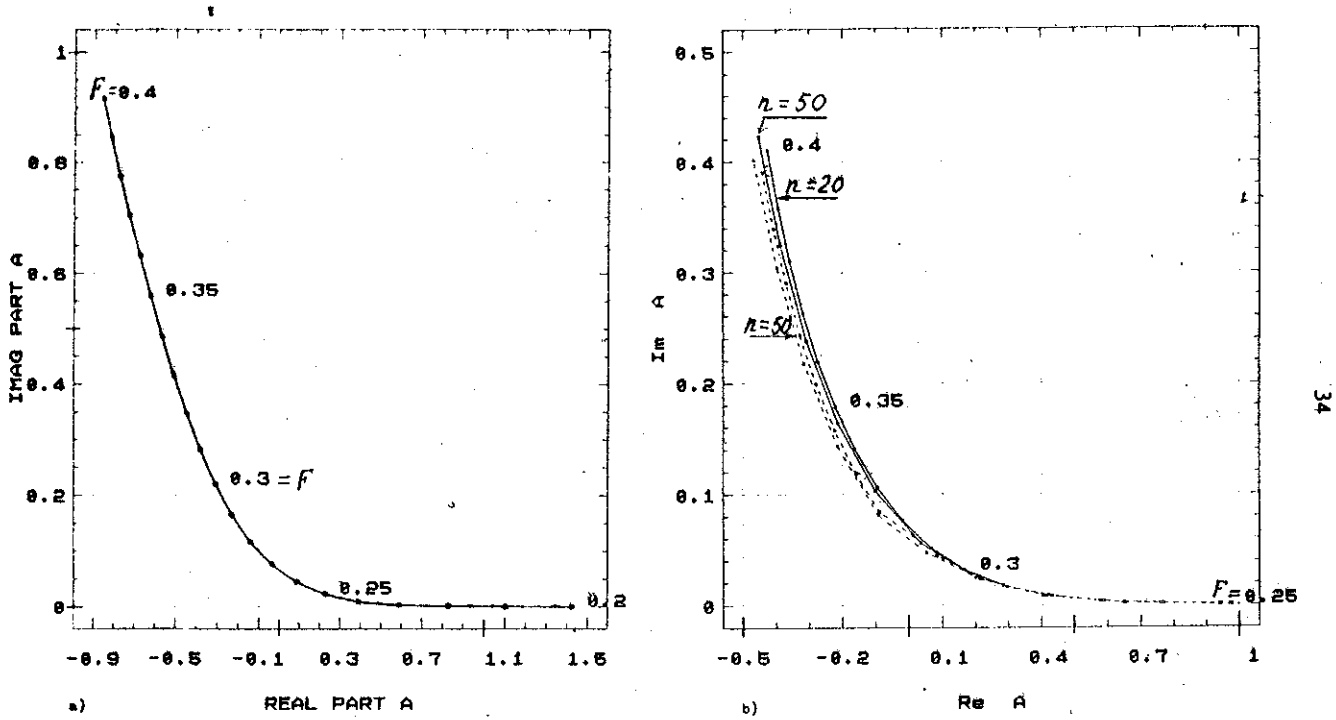

Fig.6. The parameter $a = a(F)$:
a) for $|16,1,0\rangle$ state; b) for $|n-1,0,0\rangle$ states with n=20 and 50.
The solid curves - 1/n-approximation, the dashed curves - $1/n^2$-approximation [26].

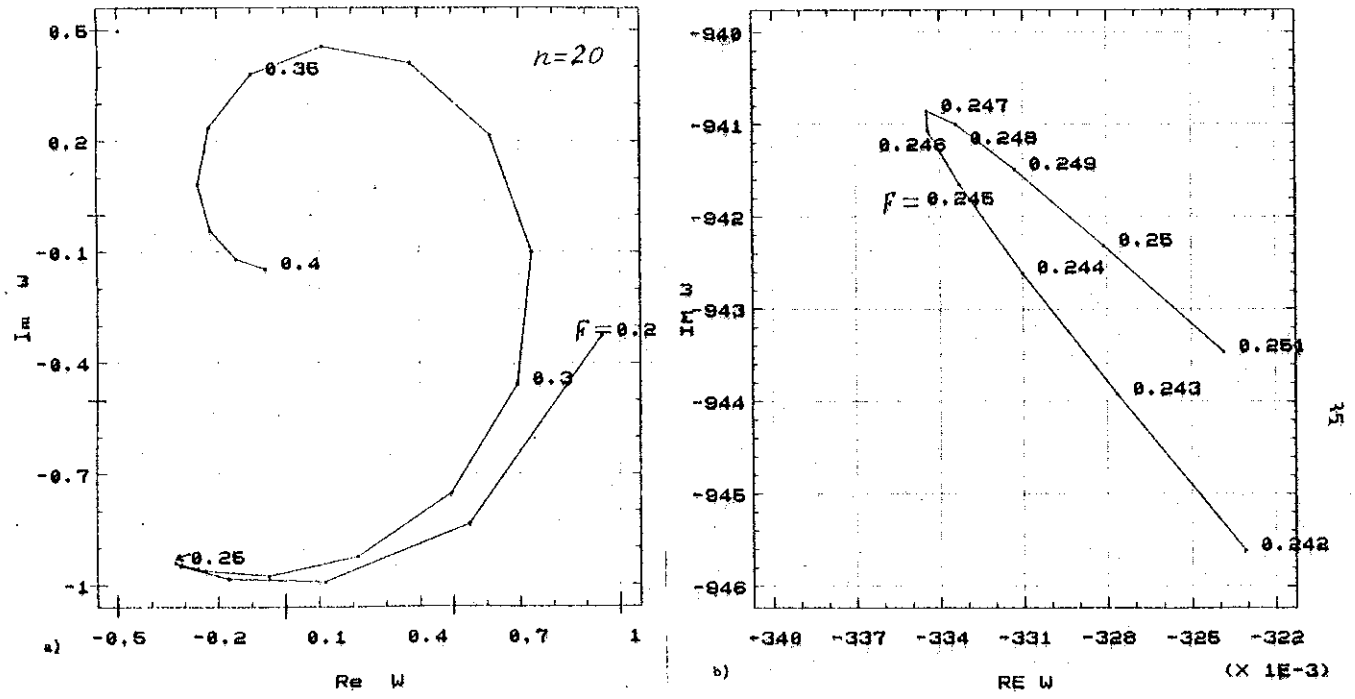

Fig.7. a) The trajectory $\omega = \omega(F)$ for $|19,0,0\rangle$ state. The value of F are marked at the curve.

b) the zoom in the preceding curve near F = 0.25.

References

1. Freeman R.R.,Economou N.P.// Phys.Rev.1979.V.A20,P.2356.
2. Luk T.S.,Di Mauro L.,Bergeman T. et al.// Phys.Rev.Lett. 1981. V.47.P.83.
3. Sandner W.,Safinya K.A.,Gallagher T.F.// Phys.Rev.1981.V.A23, P.2448.
4. Glab W.L.,Ng K.,Yao D.,Nayfeh M.H.// Phys.Rev.,1985.V.A.31, P.3677.
5. Ng K.,Yao D.,Nayfeh M.H.// Phys.Rev.,1987.V.A.35,P.2508.
6. Yao D.,Ng K.,Nayfeh M.H.// Phys.Rev.,1987.V.A36,P.4072.
7. Kolosov V.V.// Pis'ma v ZhETF,1986.V.44.P.457.
8. Weinberg V.M.,Mur V.D.,Popov V.S.,Sergeev A.V.// Pis'ma v ZhETF, 1987.V.46.P.178.
9. Popov V.S.,Weinberg V.M.M., Preprint ITEP, 1982, N 101;Doklady Akad.Nauk SSSR.1983.V.272.P.335.
10. Weinberg V.M.,Mur V.D.,Popov V.S.,Sergeev A.V.// Pis'ma v ZhETF,1986.V.44.P.9; ZhETF,1987.V.93.P.450.
11. Popov V.S.,Mur V.D.,Shcheblykin A.V.,Weinberg V.M.// Phys. Lett.1987.V.A124.P.77.
12. Weinberg V.M.,Mur V.D.,Popov V.S. et al.//Theor.Mat.Fiz.,1988, V.74.P.399.
13. Zimmerman M.L., Littman M.G.,Kash M.M. et al.// Phys.Rev.1979. V.A20.P.2251.
14. Rydberg States of Atoms and Molecules./Ed.by Stebbings R.F., Danning F.B., Cambridge Univ.Press, 1983.
15. Silverstone H.J.// Phys.Rev.,1978.V.A18.P.1853.

16. Alliluev S.P., Eletsky V.L., Popov V.S.// Phys.Lett.,1979. V.A73.P.103; 1980.V.A78.P.43.

17. Alliluev S.P.,Eletsky V.L.,Popov V.S.,Weinberg V.W.// ZhETF, 1982,V.82.P.77.

18. Privman V.L.// Phys.Rev.1980.V.A22.P.1833.

19. Popov V.S.,Mur V.D. et al. M., Preprint ITEP, 1986, N 125; 1987, N 177.

20. Bekenstein J.D., Krieger J.B.// Phys.Rev.1969.V.188.P.130.

21. Damburg R.J.,Kolosov V.V.// J.Phys.1976.V.B9.P.3149; 1978. V.B11.P.1921.

22. Fock V.A.// Zeits.Physik,1935.V.98.P.145.

23. Park D.// Zeits.Physik.1960.V.159.P.155.

24. Marinov M.S.,Popov V.S.// JàPhys.,1975.V.A8.P.1575.

25. Drukarev G.F.// ZhETF,1978.V.75.P.437.

26. Mur V.D.,Popov V.S.// Pis'ma v ZhETF,1988.V.48.P.67; ZhETF, 1988.V.94.No.10.P.125.

27. Rau A.R.P.// J.Phys.,1979.V.B12.P.L193.

28. Bateman H. Higher Transcendental Functions, v.1. McGraw-Hill, N.Y.,1953.

29. Kolosov V.V.// J.Phys.,1987,v.B20,p.2359.

В.С.Попов и др.
Эффект Штарка в сильном поле для ридберговских состояний.
Работа поступила в ОНТИ 24.10.89

Подписано к печати 9.II.89 Т20573 Формат 60x90 I/I6
Офсетн.печ. Усл.-печ.л.2,25. Уч.-изд.л.I,6. Тираж 270 экз.
Заказ 61 Индекс 3649 Цена 24 коп.

Отпечатано в ИГЭФ, II7259, Москва, Б.Черемушкинская,25

ИНДЕКС 3624

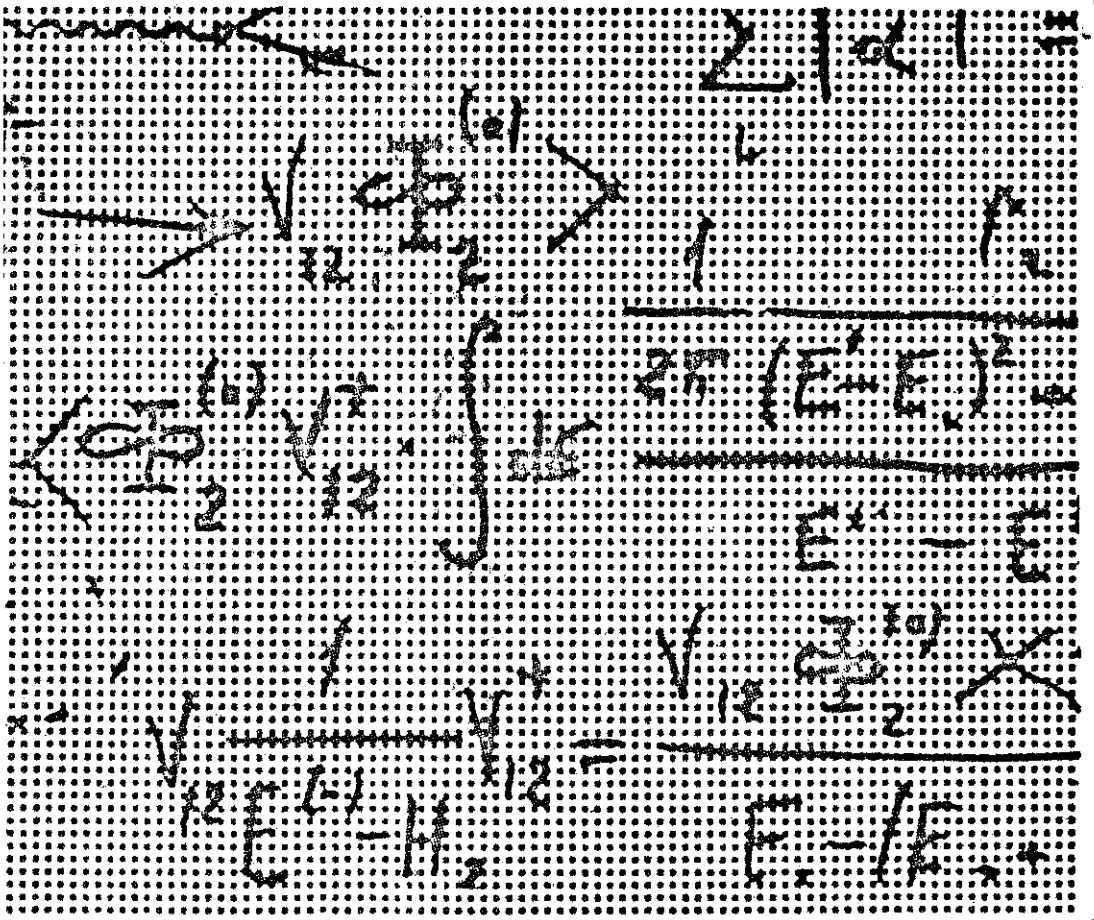

М., Препринт ИТЭФ, 1989, № 61, с.1-36